RSC Applied Interfaces

ROYAL SOCIETY OF CHEMISTRY

PAPER

View Article Online
View Journal | View Issue



Cite this: *RSC Appl. Interfaces*, 2025, **2**, 1209

# Green electrochemical sensing of ampicillin using reduced graphene oxide-modified electrodes

Dang Thi Ngoc Hoa,[a] Nguyen Duc Hong,[b] Pham Thang Long,[a] Bui Le Thanh Nhan,[a] Nguyen Ngoc Nam[a] and Do Mai Nguyen *[c]

Received 5th May 2025,
Accepted 29th May 2025

DOI: 10.1039/d5lf00127g

rsc.li/RSCApplInter

A "green" electrochemical sensor for the detection of ampicillin (AMP) was developed using a reduced graphene oxide-modified glassy carbon electrode (rGO/GCE). The sensor exhibited good performance with a linear detection range from 0.02 μM to 2.56 μM and a low detection limit of 6.75 nM. Characterization of the rGO material was carried out using Fourier-transform infrared (FT-IR) and Raman spectroscopy, confirming the successful reduction of graphene oxide and the restoration of electrical conductivity. The rGO/GCE sensor demonstrated high selectivity, minimal interference from common compounds, and good repeatability, reproducibility and long-term stability. Real-sample analysis in spiked urine achieved recovery rates of 97–103%, validated by high-performance liquid chromatography (HPLC). The results highlight the rGO/GCE sensor as a sensitive, reliable, and cost-effective platform for AMP monitoring in pharmaceutical applications.



## Introduction

The widespread presence of antibiotics in the environment has become a critical global issue, largely driven by their excessive usage and improper disposal. Among these, ampicillin or AMP, a commonly used β-lactam antibiotic, is frequently detected in various environmental matrices. Its persistence poses significant threats, including the proliferation of antibiotic-resistant bacteria and adverse ecological effects. This necessitates the development of sensitive, reliable, and cost-effective detection methods to monitor ampicillin concentrations in environmental and biological samples.[1–8]

Electrochemical sensing techniques have emerged as a promising approach for detecting antibiotics due to their high sensitivity, rapid response, and simplicity of operation. Compared to conventional methods such as high-performance liquid chromatography (HPLC), mass spectrometry (MS), or spectrophotometry, electrochemical techniques offer distinct advantages, including low cost, portability, and minimal sample preparation requirements.[9–12] Moreover, the ability to modify electrode surfaces enables the tailoring of sensor selectivity and sensitivity, making electrochemical methods particularly suitable for the detection of specific analytes such as AMP.[13–18]

In recent years, reduced graphene oxide (rGO)-modified electrodes have attracted significant attention due to their enhanced electrical conductivity, large surface area, and high electrochemical stability, which make them ideal for electrochemical sensing and energy storage applications. rGO is derived by reducing graphene oxide (GO), which involves the removal of oxygen-containing functional groups. This process restores the electrical conductivity of the material and introduces new active sites, enhancing its performance in electrochemical reactions.[11,19–22]

Compared to graphene oxide (GO), which exhibits insulating properties due to the presence of oxygenated functional groups (such as hydroxyl and carboxyl groups), rGO has superior conductivity due to the reduction process that removes some of these groups. As a result, rGO-modified electrodes typically show faster electron transfer rates, higher sensitivity, and improved electrochemical performance in various sensing applications. This enhanced conductivity makes rGO more suitable for applications like electrochemical sensors, where fast electron transfer is crucial for high-performance detection.[23–28]

Given these properties, rGO is well-suited for modifying glassy carbon electrodes (GCEs), which are widely used due to their broad potential window, low background current, and excellent chemical stability. The synergy between rGO and GCE is expected to significantly improve the sensor's performance, making it an effective platform for electrochemical detection.[12,29–36]

Recent studies have highlighted the superior electrochemical properties of rGO-modified electrodes

[a] *University of Medicine and Pharmacy, Hue University, 53000, Vietnam*
[b] *University of Agriculture and Forestry, Hue University, 53000, Vietnam*
[c] *University of Sciences, Hue University, 530000, Vietnam.*
*E-mail: nguyendomai97@gmail.com*

compared to GO and graphene. For example, Karuppasamy and his team[37] demonstrated that rGO-modified electrodes exhibit significantly higher sensitivity and faster electron transfer rates than GO, making rGO a more effective material for electrochemical sensors.[37] Additionally, rGO is shown to be more stable and efficient in various electrochemical reactions compared to graphene, which can suffer from issues related to aggregation and poor electron transfer at lower surface areas.[38]

In particular, the electrochemical behavior of rGO has been extensively investigated. Ganeshababu and his team[39] reported that sonochemical synthesized rGO exhibited improved electrochemical performance compared to both GO and graphene, owing to the uniform distribution of rGO sheets and the presence of oxygenated functional groups that aid in electron transfer.[40–42] Moreover, rGO-modified electrodes have been shown to possess excellent repeatability and reproducibility, which are critical for practical applications. This makes rGO an attractive choice for sensors designed to detect specific analytes, such as antibiotics, with high sensitivity and stability.[39,42]

Despite the increasing application of rGO-modified electrodes in sensing technologies, there is a notable lack of studies focusing on the electrochemical detection of ampicillin using this material. This gap in the literature highlights the scientific novelty of this study, which aims to optimize and evaluate the performance of an rGO-modified GCE for ampicillin detection. By leveraging the superior properties of rGO and the high sensitivity of voltammetric techniques, this research introduces a novel, efficient, and selective sensing platform.[1,10,43–45]

The distinct properties of rGO, compared to GO and graphene, make it particularly suitable for a wide range of applications in environmental monitoring and pharmaceutical analysis. For example, the study by Karthika and his team[38] demonstrated that rGO-modified electrodes provide higher electrochemical sensitivity and stability compared to graphene oxide and are more efficient in detecting environmental pollutants and pharmaceutical compounds.[38] These findings highlight the advantages of rGO in electrochemical sensing applications, especially for the detection of compounds like ampicillin.

This work systematically investigates the electrochemical behavior of AMP on the rGO/GCE using techniques such as cyclic voltammetry (CV) and differential pulse voltammetry (DPV). The key objectives of this study include the optimization of the sensor's sensitivity, selectivity, and its applicability in real-world samples. By focusing on the unique properties of rGO, such as its enhanced conductivity and high surface area, this research introduces a novel, efficient, and selective sensing platform for AMP detection. Furthermore, this study contributes to the development of advanced detection tools that are crucial for monitoring antibiotic contamination in pharmaceutical settings, addressing an urgent need for sensitive, reliable, and cost-effective analytical methods.

# Experimental

## Chemicals

All chemicals were purchased from Merck (Germany) and used without further purification. Ampicillin (99%), amoxicillin (≥98%), paracetamol (≥99%), uric acid (≥99%), sodium sulfate ($Na_2SO_4$, ≥99%), ammonium chloride ($NH_4Cl$, ≥99.5%), potassium carbonate ($K_2CO_3$, ≥99%), and calcium chloride ($CaCl_2$, ≥99%) were of analytical grade and were used in all electrochemical analyses. The Britton–Robinson buffer solutions (B–R buffer) were prepared using 0.5 M $H_3BO_3$, 0.5 M $H_3PO_4$, and 0.5 M $CH_3COOH$ solutions, covering a pH range from 2.0 to 7.0. The specific pH values of 2.0, 3.0, 4.0, 5.0, 6.0, and 7.0 were adjusted by titrating the buffer solutions with either 1 M KOH or 1 M $H_3PO_4$, depending on the required pH. This method ensures the precise pH control necessary for the electrochemical analysis of ampicillin using glassy carbon electrodes.

## Instruments

Electrochemical experiments were conducted using a CPA-HH5 computerized polarography analyzer (Vietnam). The working electrode utilized was a glassy carbon electrode (GCE) with a diameter of 2.8 mm. In contrast, an Ag/AgCl electrode (saturated KCl) was used as the reference electrode, and a platinum wire served as the auxiliary electrode.

## Preparation and modification of the working electrode *via* the electrochemical "green" method

To fabricate the reduced graphene oxide-modified glassy carbon electrode (rGO/GCE), the electrochemical reduction of graphene oxide (GO) was employed as a "green" synthesis method. This electrochemical approach was chosen for its environmental sustainability and ability to modify the electrode surface without the use of toxic reducing agents, offering a cleaner and more eco-friendly alternative to traditional chemical reduction processes.

**Preparation of GO suspension.** Graphene oxide (GO) was first dispersed in ethanol to create a stable GO suspension. The concentration of GO in the suspension was adjusted to 1 mg $mL^{-1}$. The suspension was subjected to ultrasonication for 2 hours to ensure uniform dispersion of GO and to prevent aggregation.

**Electrochemical reduction of GO.** The electrochemical reduction of GO to rGO was conducted by applying a potential of −1.2 V (*versus* Ag/AgCl) in a three-electrode electrochemical cell. A platinum wire was used as the counter electrode, and an Ag/AgCl electrode (saturated KCl) served as the reference electrode.

The reduction process was carried out in an electrolyte solution, typically a mixture of water and ethanol, to facilitate electron transfer during the reduction of GO to rGO. The process resulted in the removal of oxygen-containing groups (such as hydroxyl, epoxy, and carboxyl groups) from the GO

sheets, thereby restoring the electrical conductivity of the material and enhancing its electrochemical properties.

**Modification of GCE.** The glassy carbon electrode (GCE) was pretreated by rinsing with ethanol, followed by polishing with alumina (0.05 μm). This standard procedure ensures that the electrode surface is clean and smooth for the subsequent modification process.[38,46] However, based on recent studies, alternative pretreatment methods can further enhance the electrochemical properties of the GCE. For instance, electrochemical oxidation of the GCE surface has been shown to improve its reactivity by introducing oxygenated functional groups, which may increase the surface area and enhance the sensor's performance. This method has been demonstrated in various studies.[38,40,46]

A defined volume of the rGO suspension was then deposited onto the surface of the GCE. The electrode was allowed to dry at room temperature, ensuring that the rGO layer adhered strongly to the electrode surface. This process created the rGO/GCE, which exhibited enhanced electrochemical performance due to the high conductivity, large surface area, and abundance of active sites provided by the rGO material.[37,38]

### The preparation of the biological fluid solutions

Urine samples obtained from a cattle farm were stored in separate containers and maintained at 4 °C for 2 hours. The samples were then centrifuged at 4500 rpm for 10 minutes to separate suspended solid impurities. Each solution was filtered twice through a 0.22 μm filter before being transferred into vials and refrigerated at 4 °C.

### The practical sample preparation

Real samples were diluted using a BRBS buffer solution at pH 6. Ampicillin was determined *via* differential pulse voltammetry (DPV) with a potential scan range from −0.4 V to + 0.6 V. Spiked samples were prepared by adding 0.2 μM ampicillin to the real samples and analyzed using the same procedure. The standard HPLC method was employed to evaluate the accuracy of the analytical results obtained by the DPV method.

### The HPLC method

An accurate portion of AMP was individually transferred from its corresponding working standard solution (100 μg $mL^{-1}$) into separate sets of calibrated measuring flasks to prepare solutions having the concentration ranges of 5–40 μM of AMP. Triplicate injections were done from each of the prepared solutions. Chromatographic separation was carried out in isocratic mode on a $C_{18}$ column with a mobile phase consisting of acetonitrile : water (60/40, v/v), pH adjusted to 4.0 with orthophosphoric acid, delivered at a flow rate of 1 mL $min^{-1}$. UV scanning at 240 nm and the injection volume was 20 μL at normal room temperature. The run time was 10 min and the integrated peak area was used to determine the studied analytes.[47–49]

## Results and discussion

### Characterization

The characterization of reduced graphene oxide (rGO) was carried out using Fourier-transform infrared (FT-IR) and Raman spectroscopy, essential for understanding the material's structural properties and electrochemical performance.

FT-IR spectra of rGO (Fig. 1a): the FT-IR spectra of rGO show significant changes compared to graphene oxide (GO). The peaks corresponding to the oxygenated functional groups, such as –OH, –COOH, and –C═O, were found to be reduced or almost entirely absent. This indicates that the electrochemical reduction process successfully removed these oxygen-containing groups, restoring the graphene structure and increasing its electrical conductivity. The improvement in conductivity is crucial for electrochemical applications, as it enhances the efficiency of electron transfer at the electrode surface. This reduction process and its effects on conductivity have been confirmed in previous studies, where similar results were reported, indicating the increased conductivity of rGO after reduction.

Raman spectra of rGO (Fig. 1b): the Raman spectra of rGO exhibit two primary peaks: the D-band (~1350 $cm^{-1}$) and the G-band (~1580 $cm^{-1}$), which are characteristic of graphene-based materials.[50,51] The intensity ratio of the D-band to the G-band ($I_D/I_G$) was found to be higher for rGO than for GO, indicating an increased level of defects introduced during the reduction process.[50–53] These defects are known to provide additional active sites, which are beneficial for electrochemical applications, as they enhance the material's ability to interact with target analytes. This increased $I_D/I_G$ ratio has been shown to improve electrochemical performance by providing more active sites for electron transfer and analyte binding, as observed in several recent studies.[49–54]

The FT-IR and Raman spectra obtained in this study (Fig. 1a and b) are consistent with findings reported in recent literature.[49–54] These results demonstrate the successful electrochemical reduction of GO to rGO, which not only restores the conductivity of graphene but also introduces structural defects that improve its electrochemical properties. These enhanced properties make rGO an ideal material for electrode modification, as it facilitates rapid electron transfer and provides abundant active sites for target analyte interaction.[50–54]

The superior electrochemical behavior of the rGO-modified GCE (rGO/GCE), as demonstrated in this study, can be attributed to these structural characteristics. The electrochemical reduction process has been shown to improve both the conductivity and electrochemical activity of rGO, resulting in a significant enhancement in sensor performance.[55–58] Similar findings have recently emphasized the beneficial effects of electrochemical reduction in enhancing the performance of rGO for electrochemical sensing applications.[56,57]

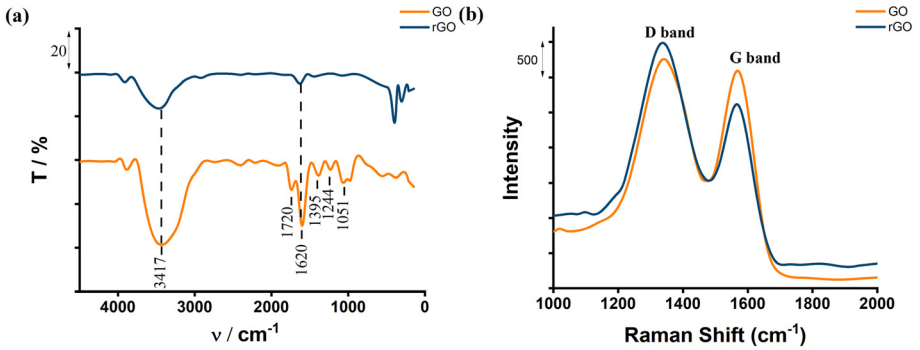


**Fig. 1** (a) FT-IR of GO and rGO; (b) Raman spectra of GO and rGO.

In conclusion, the structural characterization of rGO using FT-IR and Raman spectroscopy (Fig. 1a and b) confirms its suitability for electrochemical applications. The electrochemical reduction process not only enhances the conductivity of rGO but also introduces functional defects that improve its electrochemical stability, making it a highly effective material for electrochemical sensors.

### The electrochemical properties of AMP

The cyclic voltammograms in Fig. 2a compare the electrochemical behaviors of different electrode systems, specifically bare GCE, rGO-modified GCE (rGO/GCE), and the impact of ampicillin (AMP) presence or absence on the performance of these electrodes. The rGO/GCE with AMP (green curve) exhibits the most pronounced peak current, signifying a strong interaction between AMP and the modified electrode surface. This result highlights the enhanced sensitivity and electron transfer efficiency imparted by the rGO modification. The rGO/GCE without AMP (red curve) shows a diminished current response, demonstrating that the observed increase in the green curve is due to the specific electrochemical interaction between AMP and the rGO-modified electrode. The GCE with AMP (blue curve) reveals significantly lower peak currents than the rGO/GCE, underscoring the limited capability of the bare GCE in facilitating effective electron transfer or AMP detection. The superior performance of the rGO-modified electrode can be attributed to the high conductivity, large surface area, and rich functional groups of rGO, which enhance electron transfer kinetics and provide additional binding sites for AMP molecules. These attributes result in an amplified electrochemical signal. The rGO/GCE with AMP (green curve) represents the suitable configuration, as it provides the highest sensitivity and demonstrates the critical role of rGO in improving the detection of AMP. Therefore, rGO/GCE is chosen for the following tests.

In Fig. 2b, the bar chart represents the peak current ($I_p$) values as a function of the amount of reduced graphene oxide (rGO) used during the preparation of the modified electrode. The $I_p$ values are measured in microamperes (μA) and reflect the electrochemical activity of the electrode system. The blue bars show the corresponding Ip values for rGO amounts of 2.5 mg, 5.0 mg, 7.5 mg, 10.0 mg, and 12.5 mg.

The peak current ($I_p$) initially increases with the increasing amount of rGO, reaching a maximum of 5.0 mg. This indicates an enhancement in electrochemical activity with the incorporation of rGO due to its excellent conductivity, high surface area, and ability to facilitate electron transfer. After the peak at 5.0 mg, the Ip decreases with further increments in the rGO amount (7.5 mg, 10.0 mg, and 12.5

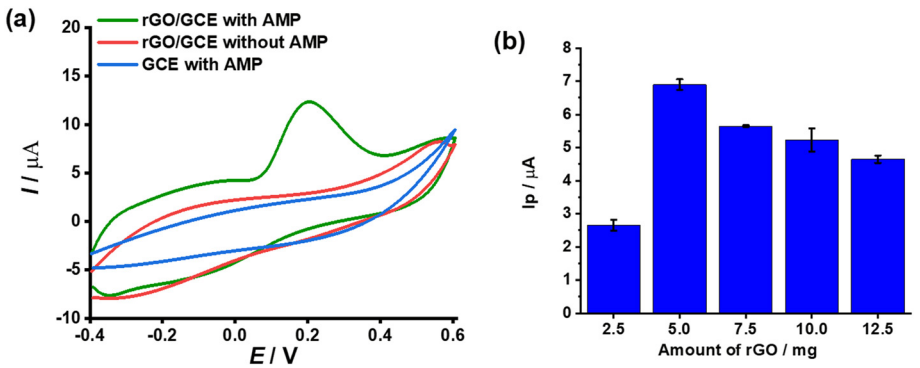


**Fig. 2** (a) CVs of AMP with several electrodes: GCE, rGO/GCE; (b) the relationship of the AMP peak current with the quantity of electrode modifier: 2.5, 5.0, 7.5, 10.0 and 12.5 μg ($C_{AMP}$ = 10 μM in BRBS 0.2 M, pH 6.0).

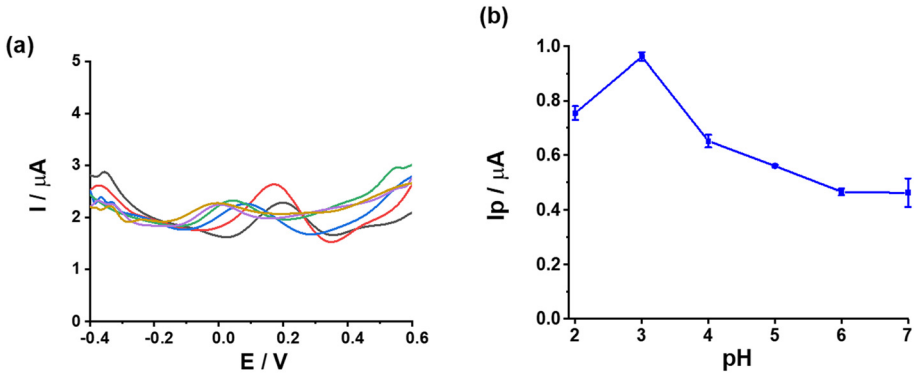


Fig. 3 (a) DPV curves of AMP with various pH values: 2, 3, 4, 5, 6 and 7; (b) plot of $I_p$ and pH.

mg). This decline suggests that excessive rGO leads to aggregation, reducing the effective surface area and active sites for the electrochemical reaction. Such aggregation likely hampers the efficient diffusion of analytes to the electrode surface, thereby diminishing the current response. The results indicate that the suitable amount of rGO for achieving the highest electrochemical performance is 5.0 mg.

### The effect of pH

The DPV curves shown in Fig. 3a illustrate the electrochemical behavior of ampicillin (AMP) across a range of pH values (2 to 7). The current response ($I$) as a function of potential ($E_p$) is presented for each pH condition, providing insights into the influence of pH on the redox process of AMP.

The intensity and sharpness of the peak current vary significantly with pH. The most pronounced peak is observed at a lower pH, particularly around pH 3, indicating enhanced electrochemical activity under acidic conditions. This suggests that AMP undergoes more efficient electron transfer at this pH, likely due to the protonation of functional groups in AMP, which facilitates the redox reaction. A noticeable shift in the peak potential occurs as the pH increases. This shift can be attributed to the involvement of protons in the redox reaction of AMP. The electrochemical process is pH-dependent, where the peak potential shifts more positively as the solution becomes less acidic. At pH values greater than 4, the peak current decreases gradually. This decline suggests that the deprotonation of AMP at higher pH values reduces its electrochemical activity, leading to a less favorable redox reaction.

The plot in Fig. 3b quantitatively represents the relationship between the peak current ($I_p$) and pH. The curve reveals a clear trend, providing additional insights into the influence of pH on the electrochemical performance of the system. The peak current is maximized at pH 3, confirming that this condition is most suitable for the electrochemical detection of AMP. At this pH, the protonation state of AMP likely enables suitable interaction with the electrode surface, enhancing the electron transfer process (Scheme 1), similar to the recently published report.[59] A significant decrease in the peak current is observed as the pH increases beyond 3. This trend supports the hypothesis that deprotonation of AMP and reduced proton availability at higher pH values diminish the redox activity, leading to a weaker electrochemical response. At neutral pH (7), the peak current reaches its lowest value, indicating minimal electrochemical activity. This is likely due to the complete deprotonation of AMP and a lack of protons participating in the redox reaction. The findings presented in Fig. 3 highlight the critical role of pH in the electrochemical detection of AMP using DPV. The redox process of AMP is proton-coupled, as reflected by the peak potential shifts and the variation in current intensity. A suitable electrochemical response is achieved at pH 3, where the peak intensity and potential are favorable for sensitive detection. This pH is recommended for further experiments and sensor optimization.

### Linear range, limit of detection (LOD) and limit of quantification (LOQ)

The DPV curves in Fig. 4a depict the electrochemical responses of ampicillin (AMP) over a concentration range

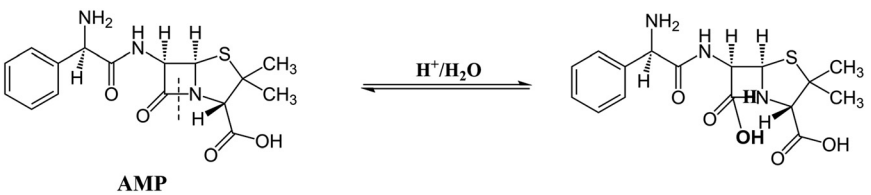


Scheme 1 Proposed mechanism for the electrochemical oxidation of AMP.[59]

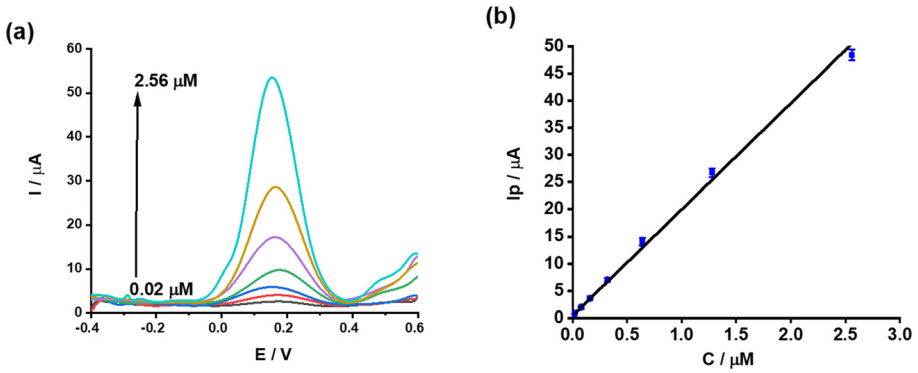


Fig. 4 (a) DPVs of AMP at several concentrations: 0.02, 0.08, 0.16, 0.32, 0.64, 1.28, 2.56 μM. (b) The plot of $I_p$ *versus* $C_{AMP,\mu M}$.

of 0.02 μM to 2.56 μM. The changes in current ($I$) with applied potential ($E$) are illustrated for different AMP concentrations, highlighting the sensitivity of the electrode system.

A gradual and well-defined peak current ($I_p$) increase is observed as the AMP concentration rises. This demonstrates the electrode's ability to detect and quantify AMP across various concentrations. The consistent and proportional increase in peak current with concentration reflects a reliable interaction between AMP and the modified electrode surface, validating the effectiveness of the sensor design. The DPV curves show sharp and well-separated peaks, particularly at higher concentrations. This indicates efficient electron transfer processes and minimal interference, essential for achieving high sensitivity and selectivity in AMP detection. The peak potential remains nearly constant across all concentrations, suggesting that the redox mechanism of AMP is unaffected by changes in concentration. This stability highlights the robustness of the electrochemical process involved.

The calibration plot in Fig. 4b presents the relationship between the peak current ($I_p$) and AMP concentration ($C_{AMP}$), with a concentration range of 0.02 μM to 2.56 μM. The plot shows a clear linear trend, providing quantitative insights into the sensor's performance.

$$I_p = (19.55 \pm 0.43)\cdot C_{AMP} + (0.43 \pm 0.04)\ R^2 = 0.998$$

The limits of detection (LOD) and quantification (LOQ) for AMP were determined to be 6.75 nM and 0.02 μM, respectively, based on the formula $3\sigma/S$ (for the LOD calculation), where $S$ represents the sensor's sensitivity, and $\sigma$ corresponds to the standard deviation of the blank signal.[60] The LOQ was subsequently calculated using the standard relation LOQ = 3 × LOD, ensuring a reliable threshold for accurate quantification of AMP in complex matrices.[60] To provide a comprehensive context for the performance of the rGO/GCE sensor, a comparison has been made with recent electrochemical systems reported for ampicillin detection between 2023 and 2025 (Table 1). Key parameters such as the limit of detection (LOD) and linear detection range have been extracted and presented for a direct benchmarking analysis.

As observed, some recently developed sensors have achieved lower detection limits, particularly those utilizing advanced nanostructured materials and molecularly imprinted polymers (MIPs). For example, a $Fe_3N$–$Co_2N$ NA@MIP-based system reported a LOD of 0.365 nM, though its linear range extended from 5.56 μM to 9.0 mM, which may not be ideal for trace-level monitoring in complex biological samples. In contrast, the proposed rGO/GCE sensor offers a balance between sensitivity and practical

Table 1 The report on LOD and the linear range of the previously published works uses several techniques

| No. | Material/electrode | Method | LOD (nM) | Linear range (μM) | Ref. |
|---|---|---|---|---|---|
| 1 | $Cu_3P$ NW/CF | Amperometric | 320 | 0.005–1000 | 61 |
| 2 | CoONR | Amperometric | 58 | 0.5–3500 | 62 |
| 3 | $Co_3N$ NW/TM | Amperometric | 50 | 0.1–2500 | 63 |
| 4 | $Co_3O_4$ MCP | Amperometric | 80 | 0.005–12 000 | 64 |
| 5 | $Fe_3N$–$Co_2N$ NA@MIP | DPV | 0.365 | 5.56–9000 | 65 |
| 6 | AuNPs/SWCNTs/GCE | DPV | 1 | 0.05–10 | 66 |
| 7 | $MoS_2$–rGO/GCE | DPV | 2.1 | 0.01–8.0 | 23 |
| 8 | AuNPs–rGO/GCE | DPV | 3.5 | 0.02–1.5 | 25 |
| 9 | MIP/SPE | SWV | 1.8 | 0.1–10.0 | 24 |
| 10 | ZnO NRs/GCE | DPV | 4.2 | 0.1–5.0 | 27 |
| 11 | rGO/GCE | DPV | 6.75 | 0.02–2.56 | This work |

Note: CF: copper foam, NR: nanorods, NW: nanowire, TM: ti-mesh, MCP: microspheres, NA: nanoarray, MIP: molecularly imprinted polymer, AuNPs: gold nanoparticles, SWCNTs: single walled carbon nanotubes.

Table 2 Influence of interferents on the oxidation of AMP

| Interferents | $C_{interferents}$ (μM) | RE (%) |
|---|---|---|
| Uric acid | 15 | 4.50 |
| Paracetamol | 20 | 3.12 |
| Amoxicillin | 10 | −2.53 |
| Chloramphenicol | 10 | −4.51 |
| $Na_2SO_4$ | 30 | −3.15 |
| $CaCl_2$ | 45 | −4.91 |
| $NH_4Cl$ | 15 | 1.78 |
| $K_2CO_3$ | 30 | −4.70 |

applicability, with a LOD of 6.75 nM and a working range from 0.02 to 2.56 μM, which aligns well with expected AMP concentrations in environmental and clinical settings.

Furthermore, the fabrication strategy employed in this work has been based on an electrochemical reduction route, eliminating the need for toxic reducing agents often used in conventional graphene oxide processing. This "green" synthesis approach not only improves environmental compatibility but also simplifies the electrode preparation process while preserving high sensitivity and selectivity.

When compared with other carbon-based systems—such as those incorporating rGO, $MoS_2$, SWCNTs, or gold nanoparticles—the proposed sensor performs comparably or more favorably in terms of both analytical figures of merit and real-sample validation. These results suggest that the proposed platform is highly competitive among current-generation electrochemical sensors for AMP and offers a sustainable, sensitive, and selective alternative for antibiotic monitoring.

## Interference

The data presented in Table 2 illustrate the influence of various interferents on the oxidation process of ampicillin (AMP), assessed through their respective concentrations (interferents) and relative errors (RE%). These findings provide critical insights into the selectivity and reliability of the electrochemical system under investigation, specifically within the context of voltammetric analysis.

From the table, it can be observed that the tested interferents, encompassing both organic compounds and inorganic salts, exhibit varying degrees of impact on the peak signal associated with AMP. Organic molecules such as uric acid, amoxicillin, chloramphenicol and paracetamol introduce moderate interference, evidenced by relative error values of +4.50%, −2.53%, −4.51% and +3.12%, respectively. This behavior could be attributed to their electroactive nature, which potentially overlaps with the oxidation potential of AMP, thereby affecting the accuracy of the measurements. Amoxicillin, structurally similar to AMP, is noteworthy for its negative interference (−2.53%), likely arising from competitive adsorption or chemical interactions at the electrode surface.

Inorganic salts, including $Na_2SO_4$, $CaCl_2$, $NH_4Cl$, and $K_2CO_3$, display varying influences. Among these, $CaCl_2$ and $K_2CO_3$ induce the highest levels of interference, with RE values of −4.91% and −4.70%, respectively, potentially due to changes in ionic strength and electrode surface interactions that affect the electron transfer kinetics. The minimal impact of $NH_4Cl$ (RE = +1.78%) suggests its compatibility with the system, likely because of its weak interaction with the electrochemical process of AMP oxidation.

The negative RE values for certain interferents indicate that suppression of the AMP oxidation signal may occur, while positive RE values reflect amplification or overlapping effects. These observations underline the necessity of meticulous optimization of the experimental conditions, including the choice of supporting electrolytes and electrode materials, to mitigate interference effects and enhance the method's selectivity.

Overall, this data highlights the robustness of the electrochemical sensor in tolerating moderate concentrations of potential interferents while underscoring areas where further refinement may be warranted to ensure reliable quantification of AMP in complex matrices. The findings contribute to a broader understanding of interferent behavior in voltammetric analyses, reinforcing the importance of comprehensive interference studies in sensor development.

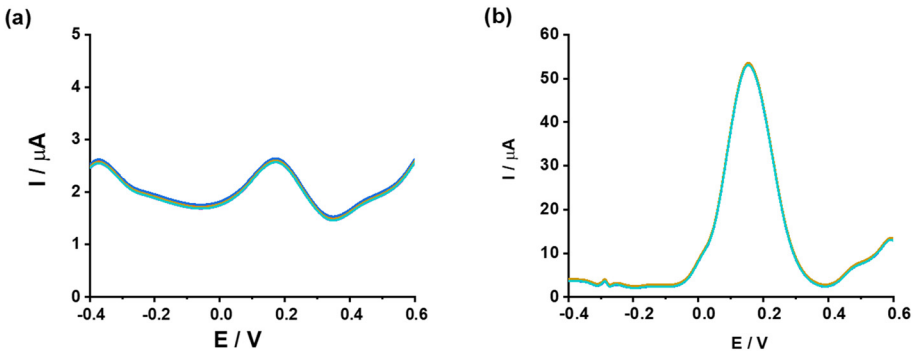


Fig. 5 Repeatability of AMP response at (a) 0.02 μM, (b) 2.56 μM. ($n$ = 9).

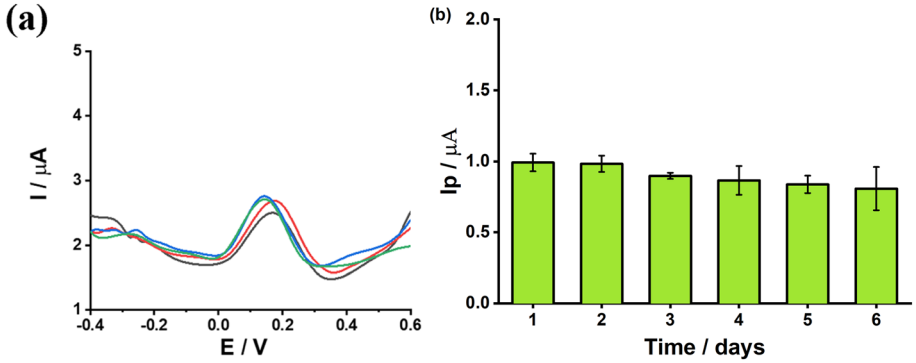


Fig. 6 (a) Reproducibility of AMP 0.02 μM in BRBS pH 3 with 4 times conductive electrode modifications, (b) peak current ($I_p$) variations of AMP across six successive modifications of rGO/GCE.

## Repeatability and reproducibility

The repeatability of the rGO/GCE electrode for DPV was evaluated by conducting 9 measurements at two different concentrations of AMP: 0.02 μM (a) and 2.56 μM (b) (Fig. 5). The calculated relative standard deviations (RSDs) were 1.33% and 0.45% for the respective TB concentrations. All these RSD values were found to be lower than half of the $RSD_{Horwitz}$ values of 16.89% and 8.14% ($RSD_{Horwitz} = 2^{1-0.5\log C}$, in that $C$, is the fraction concentration of the analysis compound).[67] These results demonstrate that the rGO/GCE electrode exhibits good repeatability and is suitable for the reliable detection of AMP across multiple concentration levels.

The reproducibility of the rGO/GCE was thoroughly investigated by employing 4 individually prepared electrodes for the determination of 0.02 μM AMP under optimized experimental conditions (Fig. 6a). The analysis revealed that the current responses exhibited an RSD of 3.7%, indicating good consistency across the measurements. The acceptable RSD obtained for these ten distinct electrodes highlights the remarkable reproducibility of the rGO/GCE in this study, demonstrating its reliability for repeated use in analytical applications. This superior reproducibility underscores the robustness and consistency of the electrode fabrication and its performance under the specified conditions.

The long-term stability of the rGO-modified glassy carbon electrode (rGO/GCE) was evaluated by monitoring the variations in peak current ($I_p$) for ampicillin (AMP) over six successive modifications, as shown in Fig. 6b. It was observed that the peak current remained stable across the six days of testing, with minimal fluctuations. The small error bars, representing the standard deviations, indicate that the electrochemical performance of the rGO/GCE was reproducible over time.

These results highlight the durability of the rGO modification, which ensures the stability of the electrode's electrochemical activity over extended periods. The consistency in peak current values suggests that the rGO layer provides a stable and reliable surface for AMP detection, with no significant loss of performance during the six-day evaluation period.

The long-term stability of the rGO/GCE is crucial for its application in continuous monitoring of AMP in real-world samples, as it guarantees that the sensor can operate effectively over prolonged periods without substantial degradation in sensitivity.

## Real sample test

The rGO/GCE was utilized for the determination of AMP in urine samples. Initially, the swine urine samples were analyzed using the DPV technique, and no electrochemical reactions were observed within the studied potential range. Based on this observation, the samples were spiked with a known concentration of AMP and subsequently analyzed with the proposed electrode *via* the DPV method. Recovery percentages ($n$ = 3) were found to range from 97% to 103% (Table 3), demonstrating that the analyzed matrices did not introduce any interference. In addition to the statistical comparison, spectral confirmation of AMP in spiked urine

Table 3 The concentrations of AMP in urine samples were measured using both DPV and HPLC techniques

| | DPV techniques | | | | HPLC techniques | |
|---|---|---|---|---|---|---|
| Sample | Original content (μM) | AMP spiked (μM) | Found (μM) | Rev (%) | AMP spiked (μM) | Found (μM) |
| #1 | —[a] | 0.2 | 0.198 ± 0.004[b] | 99 | 0.2 | 0.192 ± 0.002 |
| #2 | — | 0.2 | 0.194 ± 0.001 | 97 | 0.2 | 0.209 ± 0.001 |
| #3 | — | 0.2 | 0.207 ± 0.002 | 103 | 0.2 | 0.205 ± 0.002 |

[a] Not found. [b] Average ± standard error.

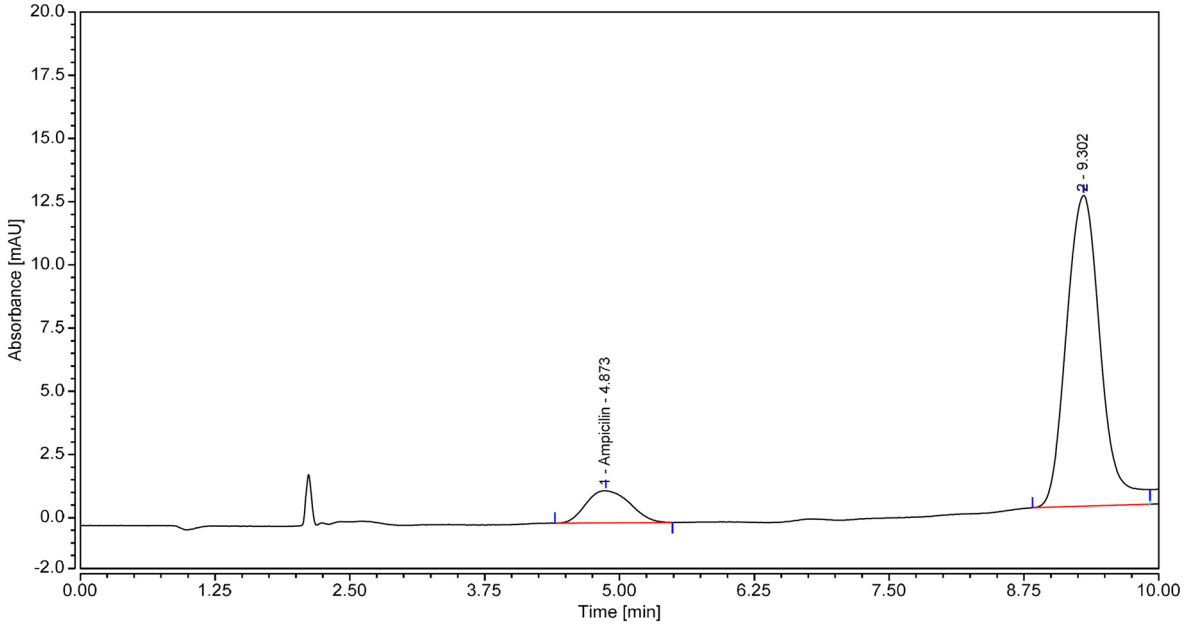


**Fig. 7** HPLC chromatogram of a spiked urine sample showing the retention peak of ampicillin at 4.873 min.

samples was conducted using HPLC. The representative chromatogram is presented in Fig. 7, where the AMP peak was observed at a retention time of 4.873 min, consistent with the standard reference. This chromatographic evidence further confirms the presence of AMP in the biological matrix and strengthens the reliability of the voltammetric approach. The inclusion of this spectral data ensures that the developed rGO/GCE platform achieves analytical validation through both electrochemical and spectroscopic methods, thereby enhancing its applicability to real-sample analysis.

For comparison, the spiked samples were also analyzed using the HPLC method, and the results obtained from both approaches are presented in Table 3. A paired-sample *t*-test, performed at $\alpha = 0.05$, indicated no statistically significant differences between the results of the proposed method and those of HPLC. This outcome ($t(2) = 0.538$, $p = 0.644 > 0.05$) confirmed the consistency and agreement between the two methods.

## Conclusions

The development of a reduced graphene oxide-modified glassy carbon electrode (rGO/GCE) for the electrochemical detection of ampicillin (AMP) has been successfully carried out in this study. Good performance has been demonstrated by the sensor, with a linear detection range from 0.02 μM to 2.56 μM and a low detection limit of 6.75 nM. The characterization of rGO, using FT-IR and Raman spectroscopy, confirmed its unique properties, including high conductivity, large surface area, and abundant active sites, which significantly contributed to the enhancement of the electrochemical performance of the rGO/GCE sensor. High selectivity, minimal interference from common compounds, and good repeatability, reproducibility and long-term stability were achieved. Real-sample analysis in spiked urine resulted in recovery rates ranging from 97% to 103%, as validated by HPLC. The rGO/GCE sensor has been shown to offer a sensitive, reliable, and cost-effective solution for the monitoring of AMP in pharmaceutical applications. Future studies are warranted to explore its potential for multi-analyte detection and its suitability for continuous monitoring in real-world applications.

## Data availability

Data are provided within the manuscript.

## Conflicts of interest

There are no conflicts of interest to declare.

## Acknowledgements

This research was funded by University of Medicine and Pharmacy, Hue University under grant number 46/24. Do Mai Nguyen was funded by the Master, PhD Scholarship Programme of Vingroup Innovation Foundation (VINIF), code VINIF.2024.TS.032.

## References

1 T. T. T. Tran, M. N. Do, T. N. H. Dang, Q. H. Tran, A. Q. Dao and Y. Vasseghian, *Environ. Res.*, 2022, **208**, 112744.
2 K. Bush, *Ann. N. Y. Acad. Sci.*, 2013, **1277**, 84–90.
3 M. Cittan, *Turk. J. Chem.*, 2021, **45**, 463–474.
4 Z. Huang, X.-D. Pan, B. Huang, J.-J. Xu, M.-L. Wang and Y.-P. Ren, *Food Control*, 2016, **66**, 145–150.

5 X. Liang, X. Liu and L. Yao, *ECS Sens. Plus*, 2022, **1**, 021401.
6 T. Q. Casuse, A. Benavidez, J. B. Plumley, L. Tsui, A.-M. Ali, J. M. Cerrato and F. H. Garzon, *ECS Sens. Plus*, 2022, **1**, 14602.
7 J. Ozhikandathil, S. Badilescu and M. Packirisamy, *ECS Sens. Plus*, 2022, **1**, 023201.
8 T. Ueda, N. Oide, K. Kamada, T. Hyodo and Y. Shimizu, *ECS Sens. Plus*, 2022, **1**, 13604.
9 Q. Wang, M. Wang, N. Zhang, X. Huang, X. Wang and S. Wang, *Microchem. J.*, 2023, **189**, 1–29.
10 N. N. Dung and D. M. Nguyen, *Hue University Journal of Science*, 2022, **131**, 89–96.
11 L. T. Thanh Nhi, L. T. Hoa, D. T. Uyen, L. H. Sinh, D. M. Nguyen, T. N. Bach, T. T. Tam Toan and D. Quang Khieu, *Vietnam J. Chem.*, 2024, **62**, 103–113.
12 D. M. Nguyen, T. T. Toan Tran, M. D. Doan, V. T. Le and Q. K. Dinh, *Chemosphere*, 2022, **303**, 135202.
13 J. Chung, L. Sepunaru and K. W. Plaxco, *ECS Sens. Plus*, 2022, **1**, 11604.
14 F. D. S. Santos, L. V. da Silva, P. V. S. Campos, C. de Medeiros Strunkis, C. M. G. Ribeiro and M. O. Salles, *ECS Sens. Plus*, 2022, **1**, 13603.
15 A. Scott, R. Pandey, S. Saxena, E. Osman, Y. Li and L. Soleymani, *ECS Sens. Plus*, 2022, **1**, 14601.
16 Y. Wu, L. Tang, L. Huang, Z. Han, J. Wang and H. Pan, *Mater. Sci. Eng. Carbon*, 2014, **39**, 92–99.
17 S. X. Luo, Y. H. Wu, H. Gou and Y. Liu, *Adv. Mater. Res.*, 2014, **850–851**, 1279–1282.
18 F. J. Pereira, M. D. Vázquez, L. Debán and A. J. Aller, *Electrochim. Acta*, 2013, **109**, 125–135.
19 Y. Li, T. Wen, C. Xue, Q. Han, Y. Wang, J. Hong, X. Zhou and H. Jiang, *Biosens. Bioelectron.*, 2013, **42**, 287–292.
20 J. V. Piovesan, E. R. Santana and A. Spinelli, *J. Electroanal. Chem.*, 2018, **813**, 163–170.
21 B. C. Lourenção, R. A. Medeiros, R. C. Rocha-Filho, L. H. Mazo and O. Fatibello-Filho, *Talanta*, 2009, **78**, 748–752.
22 L. Chen, Y. Tang, K. Wang, C. Liu and S. Luo, *Electrochem. Commun.*, 2011, **13**, 133–137.
23 L. Hou, J. Wei, C. Xiang, D. Yang and Y. Yang, *Microchim. Acta*, 2025, **192**, 1–12.
24 K. Guzelaydin, Y. Gunes, C. Anlas and M. Yildirim, *J. Vet. Sci.*, 2025, **26**, e21.
25 J. Wang, X. Li, R. Peng, J. Dong, J. Zhang, Z. Lu, X. Zhu, J. Zhang, Y. Mao and X. Liu, *Chem. Eng. J.*, 2025, 160066.
26 A. Becze, M.-A. Resz, A. Ilea and O. Cadar, *Appl. Sci.*, 2022, **12**, 9789.
27 V. Menaka and D. Geetha, *Ionics*, 2025, 1–17.
28 N. S. Md Rudin, M. A. I. Mohd Yassin and M. F. Omar, *Fullerenes, Nanotubes Carbon Nanostruct.*, 2025, 1–9.
29 T. T. T. Toan, *ECS Sens. Plus*, 2022, **1**, 31603.
30 R. Sharma, G. Lakshmi, A. Kumar and P. Solanki, *ECS Sens. Plus*, 2022, **1**, 10603.
31 D. L. Glasco, A. Sheelam, N. H. B. Ho, A. M. Mamaril, M. King and J. G. Bell, *ECS Sens. Plus*, 2022, **1**, 010602.
32 V. Chaudhary, A. K. Kaushik, H. Furukawa and A. Khosla, *ECS Sens. Plus*, 2022, **20**, 2468–2478.
33 A. Khosla, *ECS Sens. Plus*, 2022, **1**, 10001.
34 T. L. Andrew, S. Rostaminia, S. Z. Homayounfar and D. Ganesan, *ECS Sens. Plus*, 2022, **1**, 11602.
35 N. H. B. Ho, D. L. Glasco and J. G. Bell, *ECS Sens. Plus*, 2022, **1**, 20601.
36 A. Ahad and M. Tahir, *ECS Sens. Plus*, 2023, **2**, 11601.
37 P. Karuppasamy, A. Karthika, S. Senthilkumar and V. Rajapandian, *Electrocatalysis*, 2022, **13**, 269–282.
38 A. Karthika, C. Sudhakar, P. Karuppasamy, B. Tamilselvi, S. Meena, K. S. Anantharaju, K. B. Tan and H. C. A. Murthy, *Sci. Rep.*, 2024, **14**, 28714.
39 P. Karuppasamy, S. Senthilkumar, O. Ganeshbabu, S. Pitchaimuthu, M. Sennappan and V. Rajapandian, *Russ. J. Inorg. Chem.*, 2022, **67**, 2153–2165.
40 A. Karthika, P. Karuppasamy, S. Selvarajan, A. Suganthi and M. Rajarajan, *Ultrason. Sonochem.*, 2019, **55**, 196–206.
41 R. P. Vadivel, K. Venkatesh, K. Alagumalai, P. Karuppasamy, X. Arulanandam, M. A. Ansari, B. Amanulla, S. C. Kim and S. K. Ramaraj, *Ceram. Int.*, 2024, **50**, 44659–44670.
42 K. Venkatesh, B. Muthukutty, S.-M. Chen, P. Karuppasamy, A. S. Haidyrah, C. Karuppiah, C.-C. Yang and S. K. Ramaraj, *J. Ind. Eng. Chem.*, 2022, **106**, 287–296.
43 Y. Zhang, *Alexandria Eng. J.*, 2024, **96**, 185–194.
44 A. R. Marlinda, S. Sagadevan, N. Yusoff, A. Pandikumar, N. M. Huang, O. Akbarzadeh and M. R. Johan, *J. Alloys Compd.*, 2020, **847**, 156552.
45 T. T. T. Toan and D. M. Nguyen, *ECS Sens. Plus*, 2022, **1**, 21604.
46 P. Karuppasamy, D. Thiruppathi, M. Ganesan, T. Rajendran, S. Rajagopal, V. K. Sivasubramanian and V. Rajapandian, *Electrocatalysis*, 2021, **12**, 516–536.
47 J. Pacy and P. Niedzielski, *Molecules*, 2025, **30**(9), 1937.
48 M. Frigoli, M. P. Krupa, G. Hooyberghs, J. W. Lowdon, T. J. Cleij, H. Diliën, K. Eersels and B. van Grinsven, *Sensors*, 2024, **24**(17), DOI: **10.3390/s24175576**.
49 A. Becze, M. A. Resz, A. Ilea and O. Cadar, *Appl. Sci.*, 2022, **12**(19), DOI: **10.3390/app12199789**.
50 E. Adotey, A. Kurbanova, A. Ospanova, A. Ardakkyzy, Z. Toktarbay, N. Kydyrbay, M. Zhazitov, N. Nuraje and O. Toktarbaiuly, *Nanomaterials*, 2025, **15**, 1–12.
51 S. B. Singh and S. A. Dastgheib, *Carbon Trends*, 2025, **20**, DOI: **10.1016/j.cartre.2025.100511**.
52 S. Gautam, J. S. Sidhu and M. Verma, *Carbon Trends*, 2025, **19**, 100499.
53 K. Hkiri, *J. Phys.: Conf. Ser.*, 2025, **2970**, DOI: **10.1088/1742-6596/2970/1/012002**.
54 S. R. S. A. Liu X, 2024, 9, pp. 7352–7363.
55 M. Priyadarshani, K. Neha, R. Rani and R. Sharma, *Surf. Rev. Lett.*, 2025, **32**, 2450105.
56 R. Deo and M. Devi, *J. Indian Chem. Soc.*, 2025, **102**, 101507.
57 Z. Liu, X. Huang, X. Liu, J. Liu, M. Wang, T. Ding, L. Yan, Z. Zhang and G. Shi, *Small*, 2025, **21**, 2408566.
58 R. Srivastava and P. K. Singh, *Mater. Today: Proc.*, 2023, **03**, DOI: **10.1016/j.matpr.2023.02.120**.
59 I. A. Latif and S. H. Merza, *Nanosci. Nanotechnol.*, 2016, **6**, 24–33.

60 I. Taverniers, M. De Loose and E. Van Bockstaele, *TrAC, Trends Anal. Chem.*, 2004, **23**, 535–552.
61 L. Xie, A. M. Asiri and X. Sun, *Sens. Actuators, B*, 2017, **244**, 11–16.
62 C.-W. Kung, C.-Y. Lin, Y.-H. Lai, R. Vittal and K.-C. Ho, *Biosens. Bioelectron.*, 2011, **27**, 125–131.
63 F. Xie, X. Cao, F. Qu, A. M. Asiri and X. Sun, *Sens. Actuators, B*, 2018, **255**, 1254–1261.
64 C. Guo, X. Zhang, H. Huo, C. Xu and X. Han, *Analyst*, 2013, **138**, 6727–6731.
65 Z. Liu, T. Fan, Y. Zhang, X. Ren, Y. Wang, H. Ma and Q. Wei, *Microchim. Acta*, 2020, **187**, 1–9.
66 X. Shi, X. Ren, N. Jing and J. Zhang, *Anal. Lett.*, 2020, **53**, 2854–2867.
67 P. R. Dalmasso, M. L. Pedano and G. A. Rivas, *Sens. Actuators, B*, 2012, **173**, 732–736.